

## Article

# Performance Evaluation of Five GIS-Based Models for Landslide Susceptibility Prediction and Mapping: A Case Study of Kaiyang County, China

Yigen Qin <sup>1,2,3</sup> , Genlan Yang <sup>4,\*</sup>, Kunpeng Lu <sup>4</sup>, Qianzheng Sun <sup>5</sup>, Jin Xie <sup>4</sup> and Yunwu Wu <sup>6</sup>

<sup>1</sup> Guangdong Provincial Key Laboratory of Geodynamics and Geohazards, School of Earth Sciences and Engineering, Sun Yat-Sen University, Guangzhou 510275, China; qinyg3@mail2.sysu.edu.cn

<sup>2</sup> Southern Marine Science and Engineering Guangdong Laboratory, Zhuhai 519082, China

<sup>3</sup> State Key Laboratory of Earthquake Dynamics, Institute of Geology, China Earthquake Administration, Beijing 100029, China

<sup>4</sup> College of Resource and Environment Engineering, Guizhou University, Guiyang 550025, China; kplu@gzu.edu.cn (K.L.); xiejin666777888@163.com (J.X.)

<sup>5</sup> 104 Geological Brigade, Bureau of Geology and Mineral Exploration and Development of Guizhou Province, Duyun 558000, China; sqz1280143303@163.com

<sup>6</sup> Guizhou Kaiyang Economic Development Industry Investment and Development Co. Ltd., Guiyang 550300, China; zjwyw52033@126.com

\* Correspondence: glyang@gzu.edu.cn; Tel.: +86-136-0856-1277



**Citation:** Qin, Y.; Yang, G.; Lu, K.; Sun, Q.; Xie, J.; Wu, Y. Performance Evaluation of Five GIS-Based Models for Landslide Susceptibility Prediction and Mapping: A Case Study of Kaiyang County, China. *Sustainability* **2021**, *13*, 6441. <https://doi.org/10.3390/su13116441>

Academic Editors: Stefano Morelli, Veronica Pazzi and Ping Lu

Received: 10 May 2021

Accepted: 1 June 2021

Published: 5 June 2021

**Publisher's Note:** MDPI stays neutral with regard to jurisdictional claims in published maps and institutional affiliations.



**Copyright:** © 2021 by the authors. Licensee MDPI, Basel, Switzerland. This article is an open access article distributed under the terms and conditions of the Creative Commons Attribution (CC BY) license (<https://creativecommons.org/licenses/by/4.0/>).

**Abstract:** This study evaluated causative factors in landslide susceptibility assessments and compared the performance of five landslide susceptibility models based on the certainty factor (CF), logistic regression (LR), analytic hierarchy process (AHP), coupled CF–analytic hierarchy process (CF–AHP), and CF–logistic regression (CF–LR). Kaiyang County, China, has complex geological conditions and frequent landslide disasters. Based on field observations, nine influencing factors, namely, altitude, slope, topographic relief, aspect, engineering geological rock group, slope structure, distance to faults, distance to rivers, and normalized difference vegetation index, were extracted using the raster data model. The precision of the five models was tested using the distribution of disaster points for each grade and receiver operating characteristic curve. The results showed that the landslide frequency ratios accounted for more than 75% within the high and very high susceptibility zones according to the model prediction, and the AUC evaluating precision was 0.853, 0.712, 0.871, 0.873, and 0.895, respectively. The accuracy sequencing of the five models was CF–LR > CF–AHP > LR > CF > AHP, indicating that the CF–AHP and CF–LR models are better than the others. This study provides a reliable method for landslide susceptibility mapping at the county-level resolution.

**Keywords:** landslide susceptibility; certainty factor; logistic regression; analytic hierarchy process

## 1. Introduction

Landslides occur when gravity and other geologic forces move surface material downward along a slope; often, landslides cause loss of human life and property or environmental damage [1–4]. In China, many areas have been critically affected by landslides in recent years. This severely hinders the sustainable development of society and the economy and threatens the safety of people's lives and property [5–8]. Therefore, sensitivity analysis of regional landslides has important research value and practical significance for land-use planning and disaster management [9,10].

Susceptibility assessment of landslides is the first step in the hazard and risk assessment of landslides [11]. It includes summarizing the characteristics, distribution rules, spatial density, and sensitivity that influences factors of regional landslides to complete a sensitivity assessment and develop a sensitivity zoning map [12]. In the past few decades,

many prediction models have been developed to map the sensitivity of landslides. The main evaluation methods include the empirical model (fuzzy logic [13–15], analytic hierarchy process [16–21], etc.), statistical analysis model (weights of evidence [22–25], frequency ratio [19,26–29], certainty factor (CF) [18,19,30], information value model [31,32], etc.), and machine-learning models (artificial neural network [33–36], support vector machine [37–39], random forest [40,41], logistic regression [29,42–44], etc.).

Each model has its own characteristics and shortcomings, making it difficult to objectively and accurately evaluate landslide susceptibility [45]. The analytic hierarchy process (AHP), CF, and logistic regression (LR) have been applied in a large number of evaluations because of their simplicity, strong operability, and evaluation effect, but each has its own limitations [46,47]. The CF model can solve the evaluation factors based on the impact of different internal eigenvalues on the degree of liability sensitivity and by ignoring the differences in the impact of various factors on liability. The AHP cannot consider each factor's influence on different characteristic variables [46]. The LR model cannot solve the quantitative problem of each influence factor, especially in terms of consolidation issues associated with multi-source data [47]. Owing to these shortcomings, regional landslides are difficult to evaluate objectively and quantitatively. Therefore, combining the three models can better evaluate landslide susceptibility; the weight factor of the determination coefficient can be assigned to optimize the accuracy and reliability of the landslide susceptibility assessment. To ensure the feasibility of this approach, a comparative study on the advantages and disadvantages of AHP, CF, LR, CF-AHP, and CF-LR in the assessment of landslide susceptibility can provide a reference basis and comparison for the assessment of landslide susceptibility in related areas.

Landslides in China are frequent and vary in type. Southwest China, particularly Kaiyang County, Guizhou Province, which is located in the hinterland, is prone to landslide activity [48]. This region is characterized by mountainous terrain, a fragile geological environment, and frequent, heavy rainfall. The slopes in this region are vulnerable to landslides and threaten people's lives and property, hindering the social and economic development of Kaiyang County.

Assessing and managing areas that are vulnerable to landslides and mitigating the risks associated with them are necessary [49]. In this study, we consider the influence of landslides and hazard-forming factors in Kaiyang County. The analysis considers the geological environment, the spatial distribution of landslide disasters, and other relevant characteristics. Using GIS raster data, the CF, LR, AHP, CF-AHP, and CF-LR coupling models were adopted to evaluate landslide susceptibility in Kaiyang County, Guizhou Province. By comparing the different outputs of the liability evaluation methods, the results are discussed to determine which model provides the best quantitative assessment. These findings can provide theoretical guidance and technical reference for the assessment of landslide susceptibility in other regions of China at the county level.

## 2. Materials and Methods

### 2.1. Study Area

Kaiyang County is located in Guizhou Province (Figure 1a), China (26°48' N to 27°22' N and 106°45' E to 107°17' E; Figure 1b) and serves as the study area for this research. The region ranges in altitude from 515 to 1664 m (Figure 1c), with the highest elevations recorded in the southwest and the lowest in the northeast. Presinian, Cambrian, Carboniferous, Diassic, Triassic, Ordovician, Tertiary, and Quaternary strata are distributed across the county. The Baimadong Fault is the main fault in the region and is located in central Guizhou. The fold structure has the characteristics of a short and wide dome-shaped anticline and a narrow and compact linear syncline. Kaiyang County has a subtropical monsoon climate. Greater precipitation occurs in the west and south, while less precipitation occurs in the north. The Wujiang, Qingshui, and Gusa rivers are the main rivers in the study area and belong to the Yellow River network. The average annual temperature is between 10.6 and 15.30 °C. July is the hottest month (average temperature = 22.3 °C,

maximum temperature = 35.4 °C), and January is the coolest (average temperature = 2 °C, minimum temperature = −10.1 °C) [50].

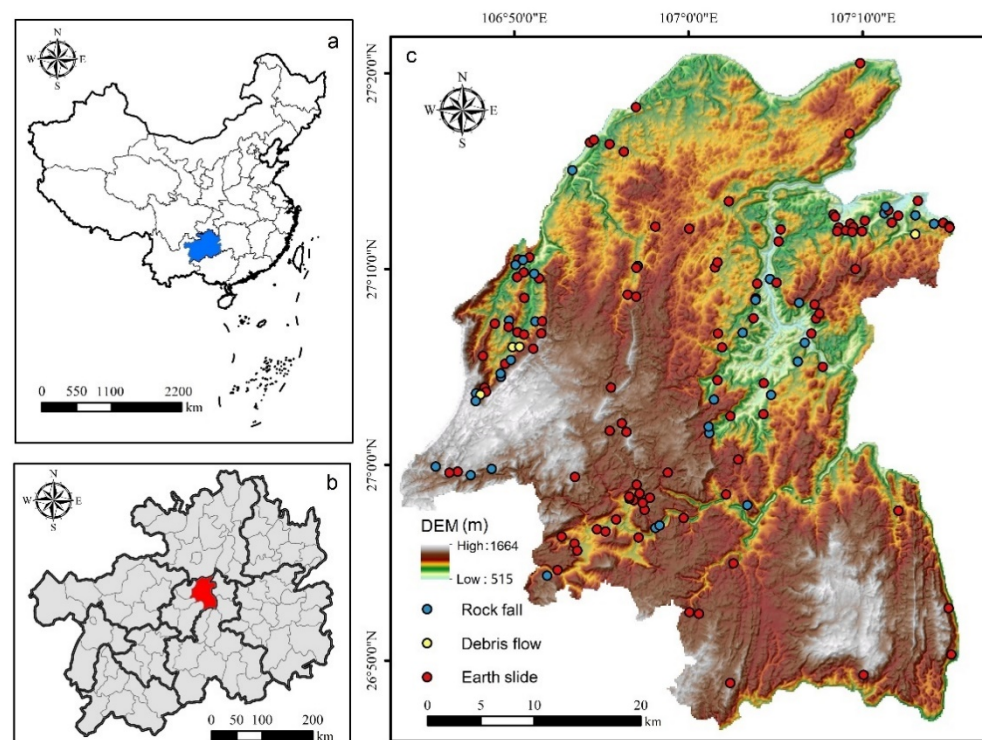


**Figure 1.** Location of the study area and landslide inventory map: (a) the geographical location of Guizhou Province in China; (b) the geographical location of Kaiyang County in Guizhou Province; and (c) the distribution of landslides and elevation in Kaiyang County.

## 2.2. Methodology

A digital elevation model (DEM) with 30 m × 30 m resolution was used to extract a set of topographic factors for the study area. The DEM was sourced from the International Scientific and Technical Data Mirror Site, Computer Network Information Center, and Chinese Academy of Sciences (<http://www.gscloud.cn>, accessed on 23 July 2010). LANDSAT-8 satellite images with a spatial resolution of 30 m × 30 m were also provided by the same institutions. Lithology maps for the study area at a scale of 1:50,000 were collected from the local Land and Resources Bureau.

## 2.3. Landslide Inventory Map

A total of 141 landslides were delineated through field investigations and landslide mapping. The landslide classification system developed by Varnes (1984) [1] was used in this study; 102 earth slides, 35 rock falls, and 4 debris flows were identified, accounting for 72%, 25%, and 3% of the total number of landslides in the region, respectively. Among these, earth slides are the most serious type of landslide in Kaiyang County (Figures 1c and 2).

## Landslide Conditioning Factors

The landslide susceptibility evaluation is based on the selection of evaluation factors [51,52]. The selection of factors that contribute to the development of landslides should be performed in combination with field investigation data. Based on the detailed investigation and study of typical disaster sites, this paper concludes that landslides in Kaiyang County are mainly controlled by topography, landform, stratigraphic lithology, geological structure, and water system dynamics. Landslides are mainly distributed alongside rivers and in areas with dense faults. Low-altitude areas recorded a significantly higher number of landslides than high-altitude areas, and 58% of landslides occurred in Cambrian strata.

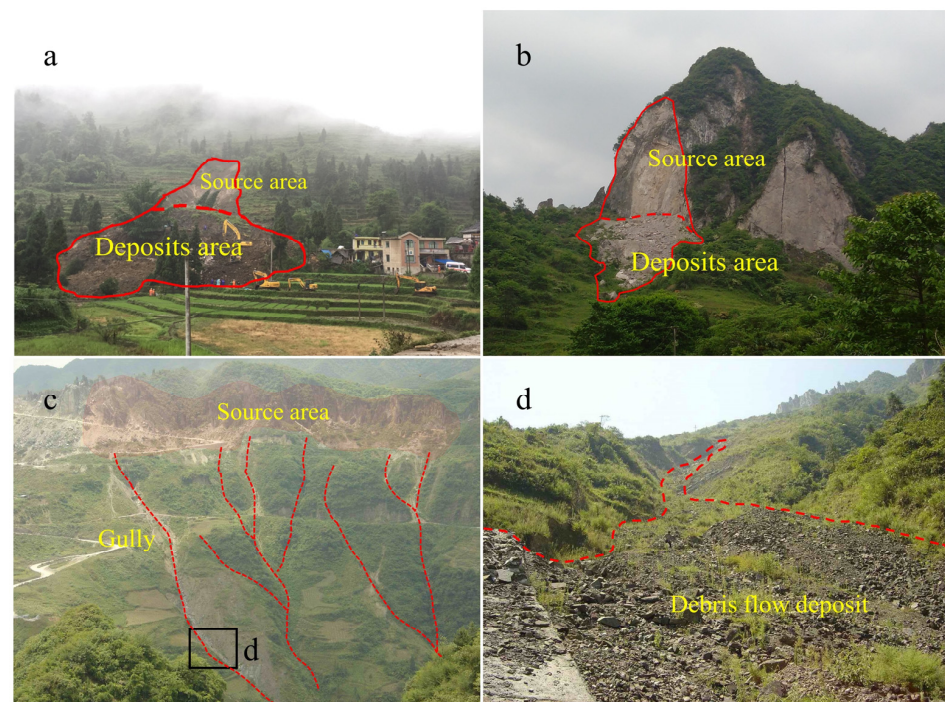


**Figure 2.** Three typical landslides that occurred in Kaiyang County of southwest China: (a) earth slide; (b) rock fall; (c) debris flow; and (d) local details of (c).

To evaluate landslide susceptibility for this study, previous research conclusions on the influencing factors of landslides were considered, as well as the nine additional factors: altitude, slope, topographic relief, slope direction, engineering rock group, slope structure, fault, drainage system, and normalized difference vegetation index (NDVI) [53,54].

#### 2.4. Correlations between Landslides and Their Conditioning Factors

Using the GIS software, the element layers were converted into raster data. Each evaluation factor layer and the landslide distribution layer were superimposed for analysis. The distribution rules of different factors and landslides were counted, and the correlation analysis between landslide pregnancy factors and landslide occurrence was carried out for the study area. Percentage of area is the ratio of a graded area to the total area of the study area, and percentage of landslide number is the ratio of the number of landslides to the total number of landslides within a certain classification. Further,  $P_n$  refers to the landslide density in the grading interval, that is, the number of landslides occurring in the unit area of the grading interval (units:  $\text{km}^2$ ).

##### 2.4.1. Altitude

Kaiyang County has an elevation of 515–1664 m, with a relative elevation difference of 1149 m. The elevation is divided into five class ranges: 515–827, 828–993, 994–1133, 1134–1287, and 1288–1664 m (Figure 3a). The statistical results of the elevation classification and spatial distribution of landslides are shown in Figure 4a. It was observed that elevation is mainly concentrated between 828 and 1287 m, accounting for 78.5% of the total area of Kaiyang County; notably, 93.8% of the disaster sites developed in areas below 1287 m. The height range of 515–827 m developed the highest density of landslides, up to  $0.14 \text{ km}^2$ .

##### 2.4.2. Slope

Slope is an important factor that affects the occurrence of landslides; it affects the direction of water flow and soil development [55]. The Kaiyang landscape is predominated by a staggered distribution of mountain basins. The range in slopes found within the region was divided into six classes:  $0\text{--}10^\circ$ ,  $10\text{--}20^\circ$ ,  $20\text{--}30^\circ$ ,  $30\text{--}40^\circ$ ,  $40\text{--}50^\circ$ , and  $>50^\circ$

(Figure 3b). The statistical results of the slope classification and spatial distribution of landslides are shown in Figure 4b. The slopes are mainly concentrated within  $0\text{--}30^\circ$ , accounting for 94.3% of the total area. Moreover, 49.6% of the slopes conducive to geological disasters appeared in the range of  $20\text{--}50^\circ$ , accounting for 20.8% of the total area. The  $30\text{--}40^\circ$  slopes contained the largest density of landslides, up to  $0.23\text{ km}^2$ , indicating that this slope range is the most prone to landslides.

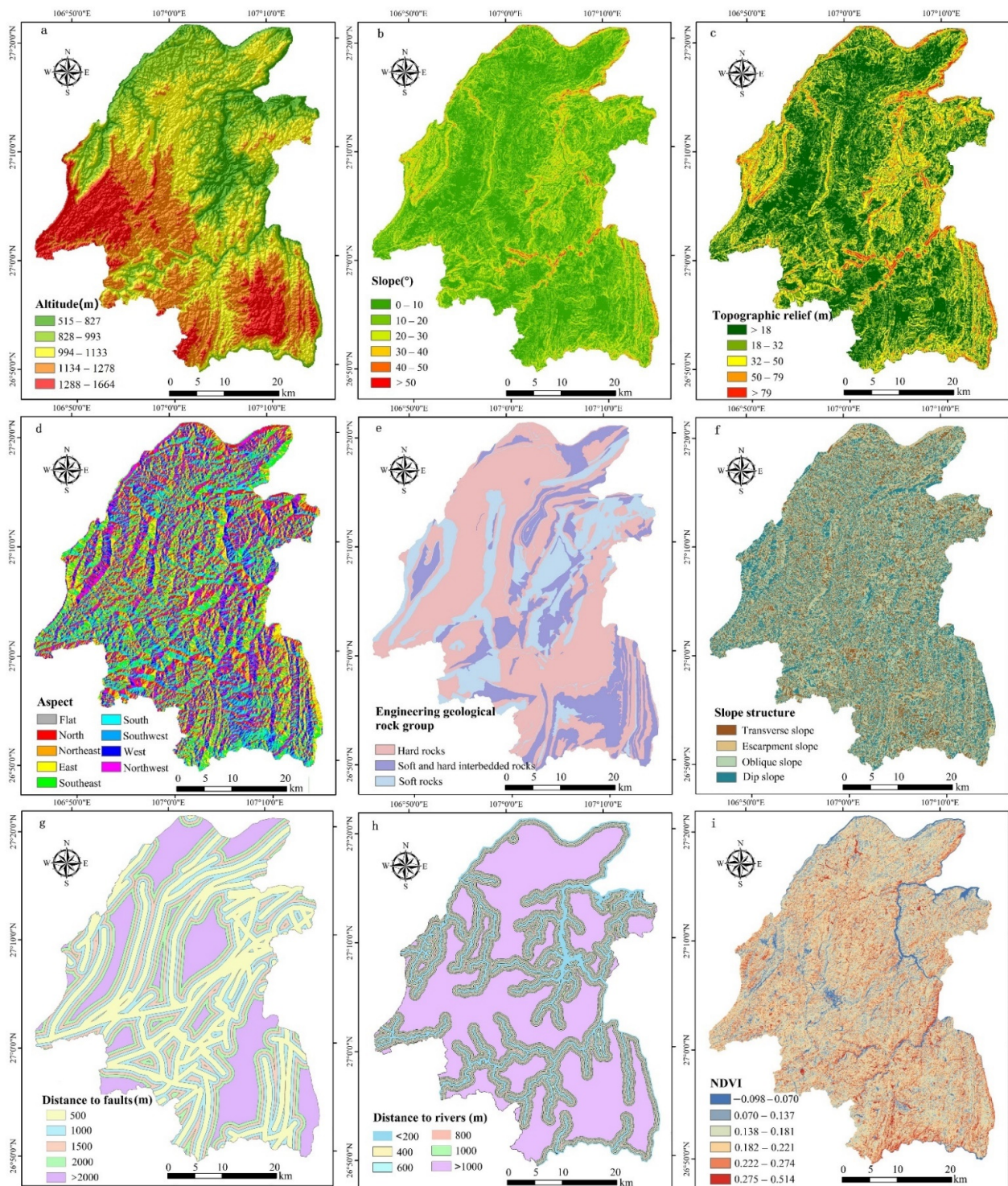


**Figure 3.** Evaluation factors of classification: (a) altitude, (b) slope, (c) topographic relief, (d) aspect, (e) engineering geological rock group, (f) slope structure, (g) distance to faults, (h) distance to rivers, and (i) NDVI.

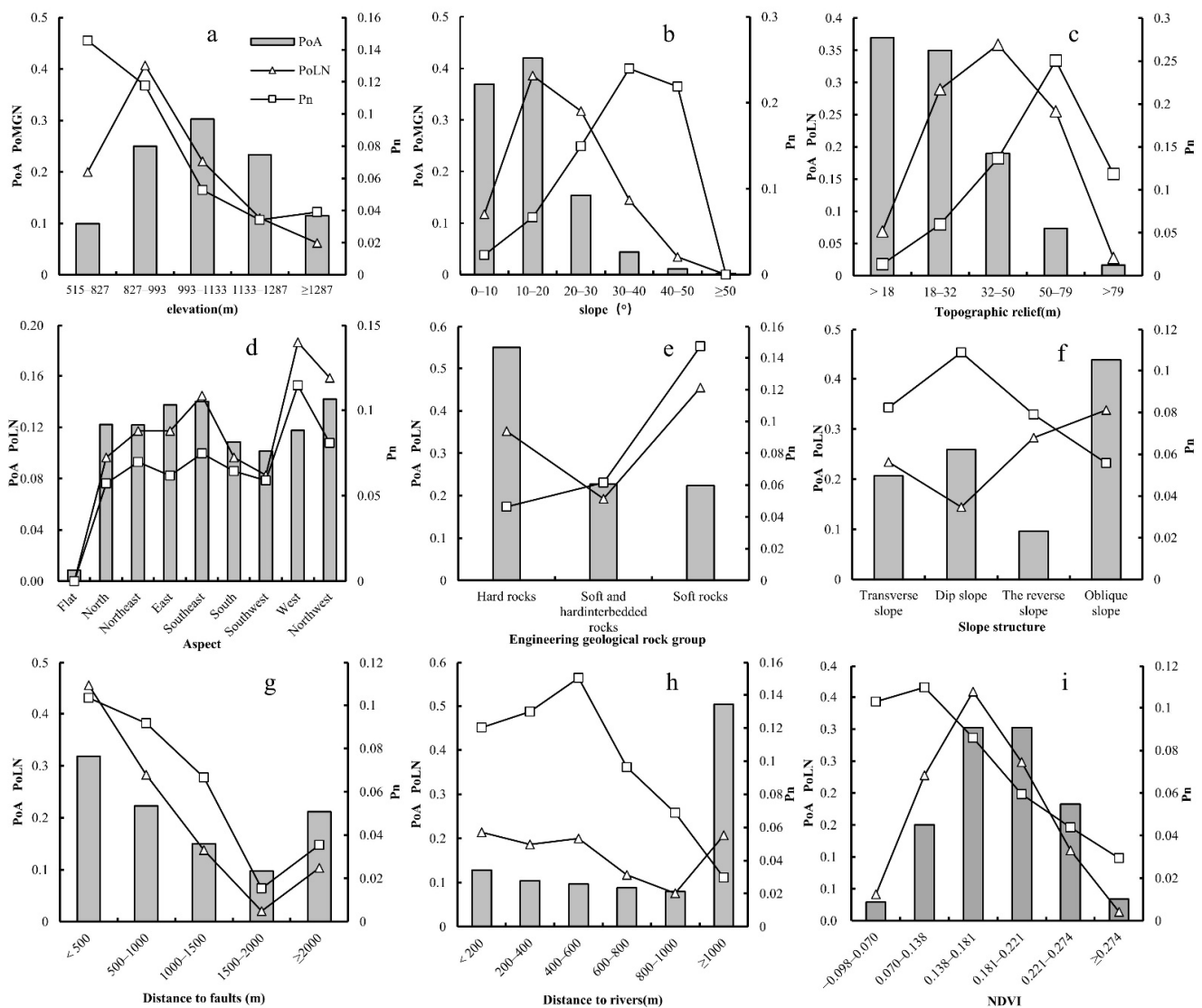


**Figure 4.** Statistical analyses of eight impact factors for the classification and spatial distribution of landslides: (a) altitude, (b) slope, (c) topographic relief, (d) aspect, (e) engineering geological rock group, (f) slope structure, (g) distance to faults, (h) distance to rivers, and (i) normalized difference vegetation index (NDVI).

#### 2.4.3. Topographic Relief

Topographic relief can reflect the macroscopic features of the terrain within a certain range [47]. Based on 30 m resolution DEM data, this study calculated the topographic relief of the study area and divided it into five classes (<18, 18–32, 32–50, 50–79, and >79 m) from Jenks natural breaks method (Figure 3c). The statistical results of the topographic relief classification and spatial distribution of landslides are shown in Figure 4c. The topographic relief is mainly concentrated at 0–79 m, accounting for 90.9% of the total area of Kaiyang County. The density of topographic relief is the highest in the >79 m topographic relief region, up to 0.25 km<sup>2</sup>, indicating that this is a highly prone area for landslides.

#### 2.4.4. Aspect

The influence of aspect on the occurrence of landslides is mainly manifested in the microclimate and the regular change of the hydrothermal ratio on the hillside [56]. The aspect factor was divided into 9 classes: (–) flat, north (0–25.5°; 315–360°), northeast (22.5–59.5°), east (59.5–135.5°), southeast (135.5–153.5°), south (153.5–215.5°), southwest (215.5–251.5°), west (251.5–298.5°), and northwest (298.5–341.5°) (Figure 3d). The statistical

results of the aspect classification and spatial distribution of landslides are shown in Figure 4d. The results show that southeast, west, and northwest aspects are most conducive to landslides in the study region, with the number of disaster points accounting for 48.9% of the total area and the area accounting for 40.0% of the total area of the study area. Among them, the aspect associated with the highest density of landslides is the west aspect, accounting for up to 0.11 km<sup>2</sup>, indicating that this aspect is the most conducive to landslides.

#### 2.4.5. Engineering Geological Rock Group

The engineering geological rock group is the material basis for landslides. The rock type and degree of hardness determine the weathering resistance of the rock mass [57]. Different lithological units were grouped into three different categories (hard rocks, soft and hard interbedded rocks, and soft rocks) based on landslide susceptibilities (Figure 3e). Hard rocks dominate in Kaiyang County (54.6% of the total area), while the density of soft rocks was the highest. The number of developmental disasters accounted for 45.5% of the total disasters, and the area accounted for 22.3% of the total area (Figure 4e).

#### 2.4.6. Slope Structure

The slope structure plays an important role in landslide distribution [54]. The types of slope structure were divided into four classes (i.e., transverse slope, reverse slope, oblique slope, and dip slope) according to the relationship between rock strata inclination and the included angle of the topographic aspect (Figure 3f). The study area was dominated by oblique slopes, accounting for 43.8% of the total area, and 85.5% of the disaster sites were developed in the transverse, normal, and oblique slopes. The density was the highest in the Shunxiang slope area, accounting for 14.4% of the total area. This area is highly prone to landslides, accounting for 9.6% of the total area (Figure 4f).

#### 2.4.7. Distance to Faults

Faults are an important influencing factor on landslide occurrence. Under the influence of faults, rock mass is broken, and joints and fissures develop, which have an adverse influence on slope deformation [58]. The distance to faults in the study area was established at a distance of 500 m (Figure 3g), and the sensitivity of each classification to landslides was statistically analyzed. The results are presented in Figure 4g. The results show that there are 65 landslides from 0 to 500 m on both sides of the fault, accounting for 46% of the total, and 36 disaster points from 500 to 1000 m away from the fault, accounting for 25.5% of the total. Generally, the landslide is negatively correlated with the distance from the fault within 1000 m. The farther the fault from the area, the lower the landslide probability.

#### 2.4.8. Distance to Rivers

Proximity to rivers can also control the distribution of landslides. Rivers have an erosion effect on the bank slope, which can change the internal stress state of the slope body and increase the possibility of bank slope instability and slippage [59]. For the rivers in the study area, buffer zones were established at intervals of 200 m (Figure 3h), and the sensitivity of the buffer zones to landslides was analyzed. The results are presented in Figure 4h. As shown in the figure, in the region within 800 m of the water system, the disaster points accounted for 71.4%, which is the area prone to landslides, accounting for 41.6% of the total area. Within the range of more than 600 m, the density showed a trend of gradual decrease with the increase in distance, indicating that the influence of the water system on landslides decreases with an increase in distance within this range.

#### 2.4.9. Normalized Difference Vegetation Index (NDVI)

The NDVI is often used to reflect human engineering activities [60]. As an index representing vegetation characteristics, vegetation coverage can represent external factors that contribute to landslides. The NDVI is divided into five class ranges: −0.098–0.070,

0.070–0.137, 0.138–0.181, 0.182–0.221, 0.222–0.274, and 0.275–0.514 (Figure 3i). Overall, vegetation coverage was relatively high in Kaiyang County. The NDVI is mainly concentrated in the range of 0.070–0.274, accounting for 93.7% of the total area; 62.8% of the disaster sites are developed in the range of NDVI = −0.098–0.181. This indicates that this area is conducive to the occurrence of landslides, accounting for 48.1% of the total area. In particular, the density of landslides is the highest in the range of 0.070–0.138, up to 0.11 km<sup>2</sup>, which is the area most prone to landslides (Figure 4i).

### 2.5. Correlations Analysis of Landslide Conditioning Factors

In the evaluation of landslide susceptibility, each conditioning factor is not independent but has a correlation with each other. If it is not dealt with, the weight of each conditioning factor may overlap with each other, leading to errors in the evaluation results. Therefore, this study used the variance inflation factor (*VIF*) and tolerance (*TOL*) to check for multicollinearity of the conditioning factors and used the Pearson correlation coefficient (*PCC*) to analyze the correlation between two conditioning factors. The *VIF* refers to the ratio of the variance between explanatory variables in the case of multicollinearity and variance in the case of no multicollinearity, so it can reflect the increased degree of variance caused by multicollinearity. Its formula is [61]

$$VIF = \frac{1}{1 - R_i^2}, \quad (1)$$

where  $R_i^2$  represents the coefficient of determination between the  $i$ th factor  $X_i$  and other factors. The tolerance and variance inflation factor are reciprocal of each other. A *VIF* > 5 or a *TOL* < 0.2 indicates a potential multicollinearity problem in the dataset [61].

Suppose the sample dataset  $(X_i, Y_j) = (x_1, y_1), (x_2, y_2), \dots, (x_n, y_n)$ . Then, the calculation formula of the correlation coefficient among evaluation factors is [62,63]

$$PCC = \frac{\sum_{i=1}^n (x_i - \bar{x}) \sum_{j=1}^n (y_j - \bar{y})}{\sqrt{\sum_{i=1}^n (x_i - \bar{x})^2 \sum_{j=1}^n (y_j - \bar{y})^2}}, \quad (2)$$

where  $x_i$  and  $y_j$  are the variable values of  $X_i$  and  $Y_j$ , respectively, and  $\bar{x}$  and  $\bar{y}$  are the mean values of  $X_i$  and  $Y_j$ , respectively. The greater the absolute value of the *PCC*, the stronger the correlation of factors. A Pearson's correlation coefficient >0.7 indicates high collinearity [64].

The multicollinearity among the remaining 9 landslide conditioning factors was identified using *TOL*, *VIF* (Table 1), and Pearson's correlation coefficient (Table 2). The results show that the highest *VIF* value is 3.943 for topographic relief, which is less than the critical value of 5. The highest correlation value (−0.267) appeared between slope structure and topographic relief, which is also less than the critical value of 0.7, indicating no multicollinearity. Therefore, all remaining 9 factors were included in the present analysis.

**Table 1.** Multicollinearity analysis for landslide conditioning factors.

Conditioning Factors	<i>TOL</i>	<i>VIF</i>
NDVI	0.936	1.068
Topographic relief	0.254	3.943
Distance to faults	0.966	1.035
Distance to rivers	0.790	1.265
Altitude	0.761	1.313
Slope	0.267	3.740
Aspect	0.955	1.048
Slope structure	0.966	1.035
Engineering geological rock group	0.899	1.112

**Table 2.** Correlation coefficients among the landslide conditioning factors.

Conditioning Factors	NDVI	Topographic Relief	Distance to Faults	Altitude	Slope	Aspect	Distance to Rivers	Slope Structure	Engineering Geological Rock Group
NDVI	1.000	−0.044	0.097	0.021	−0.027	−0.196	−0.094	−0.002	−0.114
Topographic relief		1.000	0.063	−0.218	0.204	−0.093	−0.062	−0.267	0.079
Distance to faults			1.000	−0.022	0.105	−0.082	−0.078	0.026	−0.029
Altitude				1.000	−0.112	−0.116	0.203	0.125	−0.128
Slope					1.000	−0.066	−0.065	−0.215	0.142
Aspect						1.000	−0.046	0.034	−0.001
Distance to rivers							1.000	−0.017	0.114
Slope structure								1.000	−0.097
Engineering geological rock group									1.000

## 2.6. Susceptibility Mapping Models

### 2.6.1. Certainty Factor (CF) Model

The CF model was first proposed by Shortliffe and Buchanan in 1975 [65] and improved by Heckerman (1986) [66]. The CF is a probability function used to analyze the sensitivity of various factors affecting the occurrence of events. CF is widely used in landslide susceptibility assessments. The basic assumption is that the susceptibility of a landslide can be determined based on the statistical relationship between previous landslides and datasets determined as environmental factors [29,67,68]. The equation is expressed as follows:

$$C_F = \begin{cases} \frac{PP_a - PP_s}{PP_a(1 - PP_s)}, & PP_a \geq PP_s \\ \frac{PP_a - PP_s}{PP_s(1 - PP_a)}, & PP_a < PP_s \end{cases} \quad (3)$$

where  $PP_a$  is the conditional probability of events occurring in class  $a$ ; that is, the ratio of the number of disaster points to the area in the unit of class  $a$ . Further,  $PP_s$  is the prior probability of an event occurring; that is, the ratio of the number of potential landslide points to the area in the study area.

The CF values ranged from  $-1$  to  $1$ . Positive numbers show an increase in certainty, while negative numbers correspond to a decrease in certainty. Numbers close to zero imply that the prior probability is similar to the conditional probability and do not provide any indication of certainty.

The weighted sum is carried out to obtain the landslide susceptibility index of each unit, which can be calculated by

$$I_j = \sum_i^n CF_i (i = 1, 2, \dots, n), \quad (4)$$

where  $I_j$  is the susceptibility index of the  $j$ th evaluation unit and  $CF_i$  is the CF value of each grade of the  $i$ th impact factor.

### 2.6.2. Analytic Hierarchy Process (AHP)

The AHP is a multi-index analysis and evaluation method with high precision and ease of use [69,70]. The principle is as follows: first, the evaluation factors are selected, a hierarchical structure model is established, and the relative importance of the selected evaluation factors is scored by experts. Then, the 1–9 scale method (Table 3) given by Saaty is used for scoring to construct a pair judgment matrix and test the consistency [19,71]. The consistency test index is expressed as follows:

$$CI = \frac{\lambda_{max} - n}{n - 1} \quad n > 1, \quad (5)$$

$$CR = \frac{CI}{RI}, \quad (6)$$

where *CI* is the causative index, *RI-Mean* is the random consistency index of the same order, and *CR-random* is the consistency ratio.

**Table 3.** Judgment matrix scale and its meaning [69].

Scale Values	Meaning
1	Indicates that two factors are of equal importance compared to each other
3	The former is slightly more important than the latter
5	Indicates that the former is significantly more important than the latter
7	The former is more important than the latter
9	The former is more important than the latter
2, 4, 6, 8	Represents the median value of the above adjacent judgments
The bottom	Contrary to the above effects

The judgment criterion for this study was <0.1, indicating that the test passed and the judgment matrix constructed was reasonable. The weight of each factor was calculated using the judgment matrix. The different grading state values for each factor were normalized. Finally, the susceptibility index was calculated using Equation (7) [72].

$$S_i = \sum W_i L_i, \quad (7)$$

where  $S_i$  is the AHP susceptibility index,  $W_i$  is the different grading weights of the evaluation factors, and  $L_i$  is the normalized standard value of different grades of evaluation factors.

### 2.6.3. Logistic Regression (LR) Model

The LR model is a regression analysis model of binomial categorical variables. It describes the relationship between binary dependent variables and a series of independent variables [73–76]. When conducting susceptibility assessment,  $P$  is the probability of landslide occurrence, and  $Q = (1 - P)$  is the probability of non-occurrence of a landslide. If the logarithm of  $P/Q$  is  $\ln(P/Q)$ , then the probability of landslide occurrence is regarded as the dependent variable, and the influencing factor set  $[x_1, x_2, \dots, x_n]$  is considered an independent variable. The regression Equation (8) is established as follows [77]:

$$\ln\left(\frac{P}{1-P}\right) = \alpha + \beta_1 x_1 + \beta_2 x_2 + \dots + \beta_n x_n, \quad (8)$$

where  $\alpha$  is the regression constant,  $\beta_i$  ( $i = 1, 2, \dots, n$ ) is the regression coefficient, and  $x_i$  ( $i = 1, 2, \dots, n$ ) is the index value of the impact factor. Based on this, the LR Equation (9) can be obtained:

$$\begin{cases} P = \frac{\exp(z)}{1+\exp(z)} \\ z = \alpha + \beta_1 x_1 + \beta_2 x_2 + \dots + \beta_n x_n \end{cases} \quad (9)$$

### 2.6.4. CF-AHP Integrated Model

As the deterministic coefficient model fails to consider the difference in the impact of each evaluation factor on landslide susceptibility, Fan (2017) [46] proposed a new method combining the CF and the AHP. In this method, first the CF method is used to calculate the relative weight of each evaluation factor index grading, namely, the CF value. Then, the hierarchy division of each evaluation index is carried out by combining the AHP to allocate weight scientifically and verify the reliability of weight allocation. Finally, the weight value is introduced to carry out the weighted sum of all the CF values of the impact factors, and the geological hazard susceptibility index ( $I_j$ ) of each unit is calculated using the formula [46]:

$$I_j = \sum_i^n \omega_i CF_i (i = 1, 2, \dots, n), \quad (10)$$

where  $I_j$  is the susceptibility index of the  $j$ th evaluation unit and  $\omega_i$  is the weight of the  $i$ th evaluation factor.  $CF_i$  is the CF value of each grade of the  $i$ th impact factor.

### 2.6.5. CF-LR Integrated Model

To consider the weight of each category of indicators and the weight of indicators at the same time, Cao (2020) [47] coupled the CF with LR and proposed the CF-LR integrated model. First, the CF value of each grade of evaluation factors calculated by the CF model was used as the index value of the LR analysis. Binomial LR analysis was performed to obtain the regression coefficient of each impact factor. On this basis, a LR equation was established to evaluate the landslide susceptibility [47].

## 3. Results and Discussion

### 3.1. Certainty Factor (CF) Model

The element layers were converted into raster data using GIS software, and the size of each layer cell was set to 30 m  $\times$  30 m. The layer of each evaluation factor (Figure 3) and the distribution layer of the landslides were superimposed for analysis, and a total of 2,217,519 independent attribute units were obtained.

The area of each classification and the number of landslides contained in each classification were counted, and the CF value of each classification was calculated using the CF model (Table 4). On this basis, the weighted sum is performed to obtain the geological disaster susceptibility index of each unit,  $I_j$ .

**Table 4.** Evaluation factors of the classification and CF value of each grade.

Factors	Classes	Number of Landslide	Category Area/km <sup>2</sup>	CF
Altitude (m)	515–827	29	199.08	0.542624
	828–993	59	501.26	0.415432
	994–1133	32	606.43	0.28567
	1134–1287	16	467.35	0.54544
	1288–1664	9	230.20	0.47827
Slope (°)	0–10	17	740.02	0.6985
	10–20	56	841.17	0.08543
	20–30	46	308.01	0.555807
	30–40	21	87.56	0.75283
	40–50	5	22.83	0.721837
	>50	0	4.74	−1
Topographic relief (m)	<18	10	740.84	0.82454
	18–32	42	701.80	0.18375
	32–50	52	380.38	0.507525
	50–79	37	147.57	0.766945
	>79	4	33.73	0.420283
Aspect (°)	Flat	0	17.17	−1
	North	14	245.07	0.22311
	Northeast	17	244.03	0.03983
	East	17	275.35	0.15622
	Southeast	21	280.92	0.034762
	South	14	217.62	0.11835
	Southwest	12	203.60	0.1969
	West	27	235.79	0.396943
	Northwest	23	284.75	0.112494
Engineering geological rock group	Hard rocks	51	1101.56	0.3775
	Soft and hard interbedded rocks	28	454.47	0.15811
	Soft rocks	66	448.28	0.548293

Table 4. Cont.

Factors	Classes	Number of Landslide	Category Area/km <sup>2</sup>	CF
Slope structure	Transverse slope	34	413.55	0.129424
	The reverse slope	21	193.2337	0.360400631
	Oblique slope	49	193.23	0.360401
	Dip slope	41	878.25	0.242301
Distance to faults (m)	500	66	519.28	0.090269
	1000	41	638.59	0.323431
	1500	20	447.41	0.22698
	2000	3	300.03	0.08417
	>2000	15	194.69	0.79932
Distance to rivers(m)	200	31	423.60	0.52926
	400	27	257.65	0.429814
	600	29	207.82	0.477728
	800	17	193.11	0.558687
	1000	11	176.40	0.268756
	>1000	30	159.91	0.05277
NDVI	0.098–0.070	6	1009.43	0.60723
	0.070–0.137	33	58.32	0.319929
	0.138–0.181	52	301.28	0.365997
	0.182–0.221	36	605.14	0.170441
	0.222–0.274	16	606.19	0.19041
	0.275–0.514	2	365.38	0.41277

### 3.2. AHP

We built a judgment matrix (Table 4). After calculation,  $CI = 0.144$  and  $CR = 0.0986 < 0.1$ , indicating that the construction of the judgment matrix is reasonable. The judgment matrix maximum characteristic root was determined to be  $\text{Max} = 10.152$ . Finally, the weights of each factor were determined (Table 5).

Table 5. Evaluation factor paired comparison matrix and weight.

Factor	Altitude	Slope	Aspect	Topographic Relief	Engineering Geological Rock Group	Slope Structure	Distance to Faults	Distance to Rivers	NDVI	Wi
Altitude	1	1/3	2	1/3	1/3	1/3	1/2	1/3	2	0.0533
Slope	3	1	3	2	1/3	1/2	1/2	2	3	0.1191
Aspect	1/2	1/3	1	1/3	1/4	1/3	1/2	1/3	2	0.045
Topographic relief	3	1/2	3	1	1/3	1/2	1/2	2	2	0.0996
Engineering geological rock group	3	3	4	3	1	1/3	1/3	1/3	5	0.148
Slope structure	3	2	3	2	3	1	1/2	2	3	0.1785
Distance to faults	2	2	2	2	3	2	1	2	3	0.1961
Distance to rivers	3	1/2	3	1/2	3	1/2	1/2	1	2	0.1216
NDVI	1/2	1/3	1/2	1/2	1/5	1/3	1/3	1/2	1	0.0387

### 3.3. LR Model

A total of 260 independent units (130 landslide-present pixels and 130 randomly selected landslide-absent pixels.) were randomly selected as statistical samples for susceptibility assessment. Among them, 1 indicates occurrence, and 0 indicates non-occurrence. The grading index values of nine impact factors were considered independent variables, and whether landslides occurred was regarded as the dependent variable. Binary LR analysis was conducted on the samples, and the regression results are shown in Table 6. The results of the LR analysis show that the significance of all nine impact factors was  $< 0.05$ ,

indicating that the nine factors were effective. The regression coefficients of the nine factors were substituted into the model to obtain the LR formula for susceptibility evaluation:

$$\begin{cases} P = \frac{\exp(z)}{1+\exp(z)} \\ z = 0.081 + 0.311x_1 + 0.445x_2 + 0.302x_3 \\ \quad -0.026x_4 + 0.468x_5 + 0.289x_6 + 0.384x_7 \\ \quad +0.378x_8 - 0.281x_9 \end{cases}, \quad (11)$$

where  $P$  is the probability of landslide and  $x_{1-9}$  respectively represent the index values of each grade of nine impact factors, including altitude, slope, topographic relief, aspect, engineering geological rock group, slope structure, fault, river, and NDVI.

**Table 6.** Results of logistic regression analysis.

Return to the Item	<i>B</i>	<i>SE</i>	<i>Wals</i>	<i>df</i>	<i>Sig</i>
Altitude	0.311	0.156	3.984	1	0.046
Slope	0.445	0.325	1.879	1	0.017
Topographic relief	0.302	0.304	6.940	1	0.008
Aspect	0.026	0.070	0.141	1	0.040
Engineering geological rock group	0.468	0.185	6.429	1	0.011
Slope structure	0.289	0.156	3.425	1	0.026
Distance to faults	0.384	0.119	10.442	1	0.001
Distance to rivers	0.378	0.093	16.434	1	0.000
NDVI	0.281	0.154	3.326	1	0.038
constant	0.081	1.229	0.004	1	0.948

Note: *B* represents the regression coefficient of each factor in the model, *Se* is the standard deviation, *Wals* is the chi-square, *df* is the degree of freedom, and *Sig* represents significance.

### 3.4. CF-AHP Integrated Model

AHP was used to calculate the importance of the selected index factors, and the CF method was used to calculate the CF values of different factors. Based on this, the CF weighted sum of the index factors was used to obtain the calculation formula of the sensitivity index of the evaluated region.

$$I_j = 0.0533 \times CF_1 + 0.1191 \times CF_2 + 0.0996 \times CF_3 + 0.045 \times CF_4 + 0.148 \times CF_5 + 0.1785 \times CF_6 \\ + 0.1961 \times CF_7 + 0.1216 \times CF_8 + 0.0387 \times CF_9 \quad (12)$$

### 3.5. CF-LR Integrated Model

Based on the CF model, CF values of each grade of the nine impact factors were considered independent variables, and whether landslides occurred was regarded as the dependent variable. Binary LR analysis was conducted (Table 7) to obtain the LR formula:

$$\begin{cases} P = \frac{\exp(z)}{1+\exp(z)} \\ z = 0.169 + 0.795x_1 + 0.610x_2 + 0.693x_3 \\ \quad +0.207x_4 + 1.727x_5 + 0.753x_6 + 1.584x_7 \\ \quad +1.784x_8 + 1.336x_9 \end{cases} \quad (13)$$

where  $P$  is the probability of landslide and  $x_{(1-9)}$  represents the CF values of each grade of the aforementioned nine impact factors.

**Table 7.** Results of logistic regression analysis (based on the CF value).

Return to the Item	<i>B</i>	<i>SE</i>	<i>Wals</i>	<i>df</i>	<i>Sig</i>
Altitude	0.795	0.417	3.639	1	0.036
Slope	0.610	0.497	1.507	1	0.020
Topographic relief	0.693	0.424	2.675	1	0.012
Aspect	0.207	0.803	0.067	1	0.049
Engineering geological rock group	1.727	0.466	13.727	1	0.000
Slope structure	0.753	0.803	0.878	1	0.034
Distance to faults	1.584	0.497	10.140	1	0.001
Distance to rivers	1.784	0.361	24.468	1	0.000
NDVI	1.336	0.609	4.808	1	0.028
constant	0.169	0.176	0.924	1	0.336

Note: *B* represents the regression coefficient of each factor in the model, *Se* is the standard deviation, *Wals* is the chi-square, *df* is the degree of freedom, and *Sig* represents significance.

### 3.6. Landslide Susceptibility Mapping

The grid calculator tool of GIS software was used to calculate the susceptibility index of each unit superposition. Using the Jenks natural breaks method, the susceptibility of Kaiyang County was divided into four classes: very low, low, moderate, and high (Figures 5 and 6).

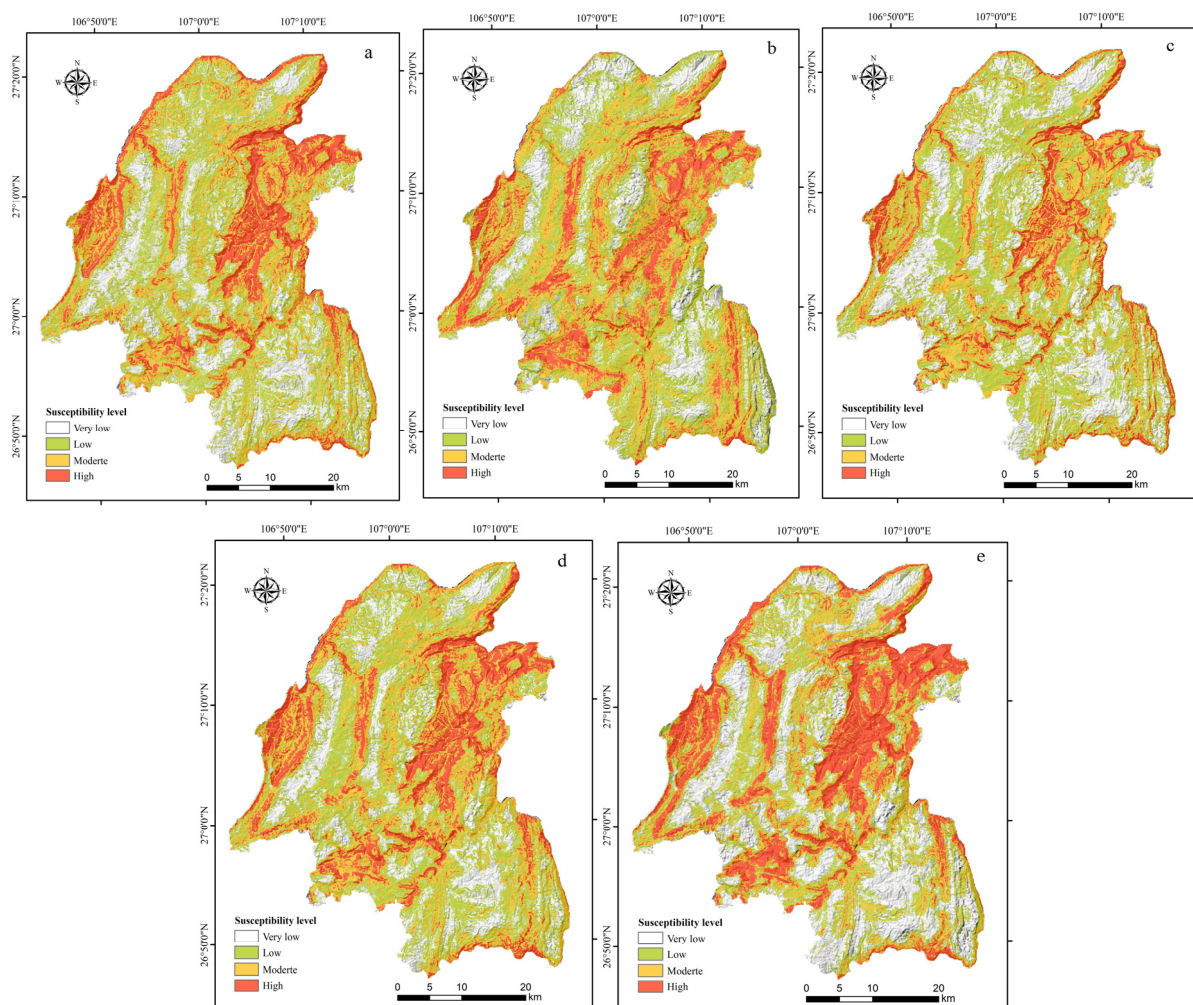


**Figure 5.** Landslide susceptibility (LS) maps of the five models: (a) the LS map of the CF model; (b) the LS map of the AHP model; (c) the LS map of the LR model; (d) the LS map of the CF-AHP model; and (e) the LS map of the CF-LR model.

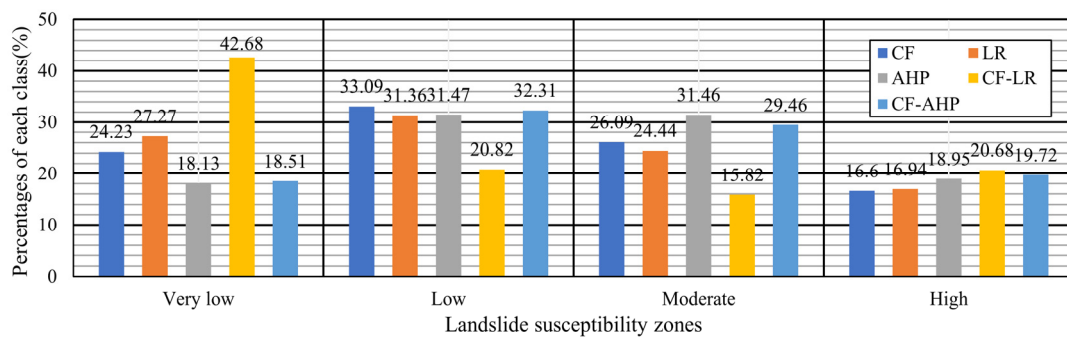


**Figure 6.** Percentages of different landslide susceptibility classes for CF, AHP, LR, CF-AHP and CF-LR models.

The resultant landslide susceptibility maps (Figure 5) suggest that the areas of high susceptibility to landslides are mainly distributed alongside rivers, in areas such as Huali Town and Jinzhong Town that were densely populated, as well as in areas with fault-concentrated belts. Areas of extremely low susceptibility to landslides are mainly distributed in Longgang Town in the south, and Nanmudu Town in the north, where the terrain is relatively flat and the geological conditions are not conducive for landslides. Figure 5 shows that the area ratios of each classification of the CF and LR model are similar. In the CF-LR model, the area of high susceptibility was 20.68%, which was higher than the 16.60% in the CF model or the 16.94% in the LR model. The area of the very low susceptibility area was 42.68%, which was higher than that of the CF model (24.23%) or the LR model (27.27%). In the CF-AHP model, the area of high susceptibility was 19.72%, which was higher than that of the CF model (16.60%) or the LR model (16.94%). The area ratio of the extremely low susceptibility area was 18.51%, which was higher than that of the CF model (24.23%) and similar to that of the AHP model (18.51%).

### 3.7. Validation of the Susceptibility Models

#### 3.7.1. Distribution of Landslides

The accuracy of the evaluation results can be tested by counting the percentage of the number of landslides in each susceptibility classification in the total number of landslides. The statistical results (Figure 7) show that 89.11% and 86.90% of landslides in the CF-AHP and CF-LR models fall in the medium to high-susceptibility areas, respectively; these values are higher than those recorded by the CF-AHP (82.89%), LR (80.65%), and AHP (76.19%) models, respectively. The results show that the evaluation results using the CF-AHP and CF-LR models are more reasonable than the CF, AHP, and LR models.

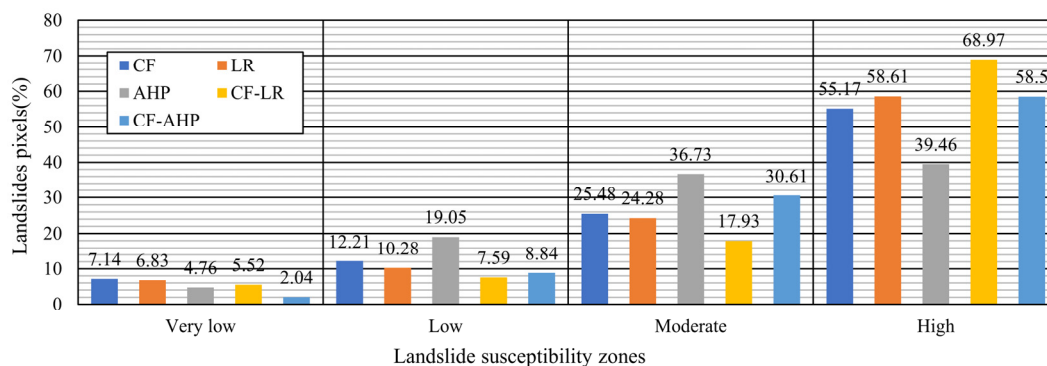


**Figure 7.** Verification of landslide susceptibility maps for CF, AHP, LR, CF-AHP, and CF-LR models.

#### 3.7.2. Receiver Operating Characteristic Curves

The receiver operating characteristic curve (ROC) is a common method for accuracy verification of landslide susceptibility evaluation, and it is widely used in the accuracy verification of landslide susceptibility evaluation. To show the evaluation effect more

clearly, the area under the receiver operating curve (AUC) is typically used as an objective and quantitative evaluation index to measure the accuracy of the model's prediction [32]. The AUC value ranges between 0 and 1; the closer it is to 1, the higher is the prediction accuracy. The ROC test results for the five models in this study are shown in Figure 8. The test results show that the AUC values of the CF, AHP, LR, CF-AHP, and CF-LR models were 0.853, 0.712, 0.871, 0.873, and 0.895, respectively. With the exception of the AHP model, the AUC value of the other models is greater than 0.75, indicating that these models accurately evaluate the landslide susceptibility. The accuracy of the five models ranged from the highest to the lowest as follows: CF-LR, CF-AHP, LR, CF, and AHP. The success rates of the CF-AHP and CF-LR models were higher than those of the models using CF-AHP, AHP, and LR, respectively.

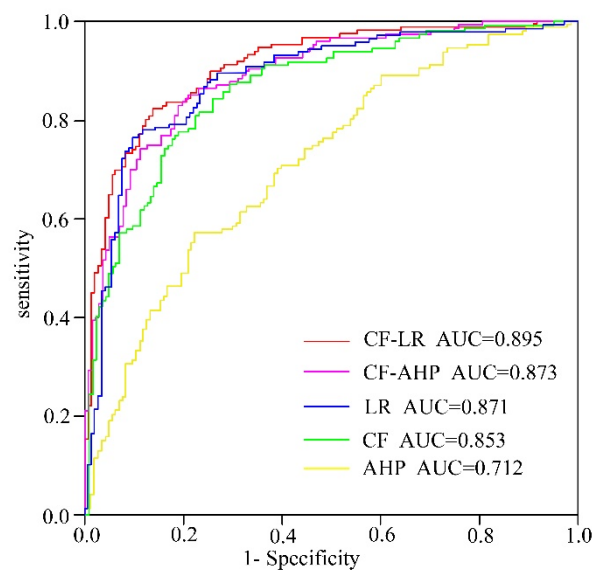


**Figure 8.** Comparison of receiver operating characteristic (ROC) curves and area under the curve (AUC) values.

### 3.8. Uncertainty Analysis

As for landslides, there are some uncertainties in landslide susceptibility evaluation because of the complexity of the forming mechanism, the uncertainty of obtaining relevant data such as landslide cataloging, and the difference of prediction principles of different analysis models. For the AHP method, the rating system is mainly based on expert opinions, which is a subjective method and may have great defects. When making grading decisions on slopes, experienced experts generally assign a relatively high vulnerability index to a high slope and a relatively low vulnerability index to a low slope. In fact, the Pn values of landslide points in the six classes are 0.0229 (0–10°) and 0.0665 (10–20°), 0.1493 (20–30°), 0.2398 (30–40°), 0.2189 (40–50°), and 0 (>50°), respectively. The number of landslides in >50° region is not higher than those in 30–40° and 40–50° regions. Therefore, it is difficult to estimate the actual weight of factors when only starting from professional knowledge and general experience, and one cannot comprehensively analyze the actual situation. For the CF and LR models, the accuracy is mainly affected by the unbalanced sample sets. Landslide and non-landslide points are strongly unbalanced data sets. When using the sampling method to select non-landslide points, it is difficult to directly determine the specific location of non-landslide areas; therefore, there are differences in the selection methods of non-landslide points. In this study, through random sampling in the whole area, it is difficult to obtain good non-landslide points, which affects the accuracy of the model to some extent. These problems need to be solved in future research.

#### 4. Conclusions

Although past studies have individually applied the AHP, CF, LR, CF-AHP, and CF-LR methods to examine landslide distribution and susceptibility characteristics, these methods have not previously been compared for accuracy. This study applied all five of these modeling approaches to the same area (Kaiyang County, China) to map landslide susceptibility and then compared the results obtained from the analyses. Five models were used to produce landslide maps, and the suitability of each model was evaluated using the area under the curve method and by comparing the maps with known landslide locations. The accuracies of the landslide maps produced by the CF, AHP, LR, CF-AHP, and CF-LR methods were 0.853, 0.712, 0.871, 0.873, and 0.895, respectively. The success rates of the CF-AHP and CF-LR models were higher than those of the CF, AHP, and LR models. By combining CF with the LR method, or CF with the AHP method, the shortcomings of the CF model were resolved, and the quadratic LR calculation of the landslide index factor was realized. The ROC precisions of the CF-AHP and CF-LR models were 0.838 and 0.836, respectively. Compared with the single AHP and CF models, the accuracy of landslide susceptibility assessment can be improved by approximately 8%, indicating that the CF-AHP and CF-LR models have a higher success rate than the single AHP and CF models in the assessment of landslide hazard susceptibility; these findings provide a reliable way to improve the assessment process of landslide hazard susceptibility in the Kaiyang region and elsewhere.

The comparison results of the present study indicate that except for the AHP model, the AUC value of all the other models was greater than 0.75, and the frequency ratio of extremely vulnerable areas and highly vulnerable areas accounted for more than 80% of the total frequency ratio. This indicates that the landslide susceptibility of Kaiyang County could be accurately evaluated using these methods.

By comparing and analyzing the value of CF and regression coefficient B of each characteristic value of the nine factors, it can be observed that the three influencing factors, namely formation lithology, distance from fault, and distance from the water system, contribute significantly to landslide susceptibility. In particular, landslides are more likely to occur within 1000 m of a fault, 800 m of a water system, and in lithologies of soft rock formation.

Landslide susceptibility maps provide decision support to planners and engineers who must choose suitable locations to implement development action plans. The landslide susceptibility maps produced in this study can aid planners and engineers in future development and land-use planning for Kaiyang County.

**Author Contributions:** All authors conceptualized the main research purpose of the paper. Y.Q. and G.Y. performed the analysis, prepared the data, tables, and figures, and wrote the majority of the first draft of the paper. K.L., Q.S., J.X. and Y.W. contributed with paper review and editing. All authors have read and agreed to the published version of the manuscript.

**Funding:** This study was supported by the Basic research program of Guizhou Provincial Science and Technology Foundation (ZK[2021] Basic 200).

**Institutional Review Board Statement:** Not applicable.

**Informed Consent Statement:** Not applicable.

**Acknowledgments:** The authors are grateful to editors and reviewers for their enthusiastic help and valuable comments.

**Conflicts of Interest:** The authors declare no conflict of interest.

#### References

1. Varnes, D.J. Landslide hazard zonation: A review of principles and practice. *Nat. Hazards* **1984**, *3*, 63. [[CrossRef](#)]
2. Jeong, S.; Kassim, A.; Hong, M.; Saadatkah, N. Susceptibility Assessments of Landslides in Hulu Kelang Area Using a Geographic Information System-Based Prediction Model. *Sustainability* **2018**, *10*, 2941. [[CrossRef](#)]

3. Nguyen, V.-T.; Tran, T.H.; Ha, N.A.; Ngo, V.L.; Nadhir, A.-A.; Tran, V.P.; Duy Nguyen, H.; Ma, M.; Amini, A.; Prakash, I.; et al. GIS Based Novel Hybrid Computational Intelligence Models for Mapping Landslide Susceptibility: A Case Study at Da Lat City, Vietnam. *Sustainability* **2019**, *11*, 7118. [[CrossRef](#)]
4. Harrison, J.F.; Chang, C.-H. Sustainable Management of a Mountain Community Vulnerable to Geohazards: A Case Study of Maolin District, Taiwan. *Sustainability* **2019**, *11*, 4107. [[CrossRef](#)]
5. Lin, G.-W.; Chen, H.; Shih, T.-Y.; Lin, S. Various links between landslide debris and sediment flux during earthquake and rainstorm events. *J. Asian Earth Sci.* **2012**, *54–55*, 41–48. [[CrossRef](#)]
6. Ma, T.; Li, C.; Lu, Z.; Bao, Q. Rainfall intensity–duration thresholds for the initiation of landslides in Zhejiang Province, China. *Geomorphology* **2015**, *245*, 193–206. [[CrossRef](#)]
7. Wang, L.-J.; Guo, M.; Sawada, K.; Lin, J.; Zhang, J. Landslide susceptibility mapping in Mizunami City, Japan: A comparison between logistic regression, bivariate statistical analysis and multivariate adaptive regression spline models. *Catena* **2015**, *135*, 271–282. [[CrossRef](#)]
8. Xu, C.; Xu, X.; Shyu, J.B.H.; Zheng, W.; Min, W. Landslides triggered by the 22 July 2013 Minxian–Zhangxian, China, Mw 5.9 earthquake: Inventory compiling and spatial distribution analysis. *J. Asian Earth Sci.* **2014**, *92*, 125–142. [[CrossRef](#)]
9. Fell, R.; Corominas, J.; Bonnard, C.; Cascini, L.; Leroi, E.; Savage, W.Z. Guidelines for landslide susceptibility, hazard and risk zoning for land use planning. *Eng. Geol.* **2008**, *102*, 85–98. [[CrossRef](#)]
10. Saha, A.K.; Gupta, R.P.; Sarkar, I.; Arora, M.K.; Csaplovics, E. An approach for GIS-based statistical landslide susceptibility zonation? with a case study in the Himalayas. *Landslides* **2005**, *2*, 61–69. [[CrossRef](#)]
11. Trigila, A.; Iadanza, C.; Esposito, C.; Scarascia-Mugnozza, G. Comparison of Logistic Regression and Random Forests techniques for shallow landslide susceptibility assessment in Giampilieri (NE Sicily, Italy). *Geomorphology* **2015**, *249*, 119–136. [[CrossRef](#)]
12. Jiang, W.; Rao, P.; Cao, R.; Tang, Z.; Chen, K. Comparative evaluation of geological disaster susceptibility using multi-regression methods and spatial accuracy validation. *J. Geogr. Sci.* **2017**, *27*, 439–462. [[CrossRef](#)]
13. Champati ray, P.K.; Dimri, S.; Lakhera, R.C.; Sati, S. Fuzzy-based method for landslide hazard assessment in active seismic zone of Himalaya. *Landslides* **2006**, *4*, 101–111. [[CrossRef](#)]
14. Kanungo, D.P.; Arora, M.K.; Gupta, R.P.; Sarkar, S. Landslide risk assessment using concepts of danger pixels and fuzzy set theory in Darjeeling Himalayas. *Landslides* **2008**, *5*, 407–416. [[CrossRef](#)]
15. Pradhan, B. Application of an advanced fuzzy logic model for landslide susceptibility analysis. *Int. J. Comput. Intell. Syst.* **2010**, *3*, 370–381. [[CrossRef](#)]
16. Chen, W.; Li, W.; Chai, H.; Hou, E.; Li, X.; Ding, X. GIS-based landslide susceptibility mapping using analytical hierarchy process (AHP) and certainty factor (CF) models for the Baozhong region of Baoji City, China. *Environ. Earth Sci.* **2015**, *75*, 63. [[CrossRef](#)]
17. Demir, G.; Aytakin, M.; Akgün, A.; İkozler, S.B.; Tatar, O. A comparison of landslide susceptibility mapping of the eastern part of the North Anatolian Fault Zone (Turkey) by likelihood-frequency ratio and analytic hierarchy process methods. *Nat. Hazards* **2013**, *65*, 1481–1506. [[CrossRef](#)]
18. Shahabi, H.; Khezri, S.; Ahmad, B.B.; Hashim, M. Landslide susceptibility mapping at central Zab basin, Iran: A comparison between analytical hierarchy process, frequency ratio and logistic regression models. *Catena* **2014**, *115*, 55–70. [[CrossRef](#)]
19. Yalcin, A.; Reis, S.; Aydinoglu, A.C.; Yomralioglu, T. A GIS-based comparative study of frequency ratio, analytical hierarchy process, bivariate statistics and logistics regression methods for landslide susceptibility mapping in Trabzon, NE Turkey. *Catena* **2011**, *85*, 274–287. [[CrossRef](#)]
20. Hepdeniz, K. Using the analytic hierarchy process and frequency ratio methods for landslide susceptibility mapping in Isparta-Antalya highway (D-685), Turkey. *Arab. J. Geosci.* **2020**, *13*. [[CrossRef](#)]
21. Senouci, R.; Taibi, N.-E.; Teodoro, A.C.; Duarte, L.; Mansour, H.; Yahia Meddah, R. GIS-Based Expert Knowledge for Landslide Susceptibility Mapping (LSM): Case of Mostaganem Coast District, West of Algeria. *Sustainability* **2021**, *13*, 630. [[CrossRef](#)]
22. Chen, W.; Zhang, G.-N.; Xu, L.-M.; Gu, R.; Xu, Z.-H.; Wang, H.-J.; He, Z.-B. Low temperature processed, high-performance and stable NiOx based inverted planar perovskite solar cells via a poly(2-ethyl-2-oxazoline) nanodots cathode electron-extraction layer. *Mater. Today Energy* **2016**, *1–2*, 1–10. [[CrossRef](#)]
23. Oh, H.-J.; Lee, S. Landslide susceptibility mapping on Panaon Island, Philippines using a geographic information system. *Environ. Earth Sci.* **2011**, *62*, 935–951. [[CrossRef](#)]
24. Ozdemir, A.; Altural, T. A comparative study of frequency ratio, weights of evidence and logistic regression methods for landslide susceptibility mapping: Sultan Mountains, SW Turkey. *J. Asian Earth Sci.* **2013**, *64*, 180–197. [[CrossRef](#)]
25. Sharma, M.; Kumar, R. GIS-based landslide hazard zonation: A case study from the Parwanoo area, Lesser and Outer Himalaya, H.P. India. *Bull. Eng. Geol. Environ.* **2008**, *67*, 129–137. [[CrossRef](#)]
26. Juliev, M.; Mergili, M.; Mondal, I.; Nurtaev, B.; Pulatov, A.; Hübl, J. Comparative analysis of statistical methods for landslide susceptibility mapping in the Bostanlik District, Uzbekistan. *Sci. Total Environ.* **2019**, *653*, 801–814. [[CrossRef](#)] [[PubMed](#)]
27. Yan, F.; Zhang, Q.; Ye, S.; Ren, B. A novel hybrid approach for landslide susceptibility mapping integrating analytical hierarchy process and normalized frequency ratio methods with the cloud model. *Geomorphology* **2019**, *327*, 170–187. [[CrossRef](#)]
28. Bostjančić, I.; Filipović, M.; Gulam, V.; Pollak, D. Regional-Scale Landslide Susceptibility Mapping Using Limited LiDAR-Based Landslide Inventories for Sisak-Moslavina County, Croatia. *Sustainability* **2021**, *13*, 4543. [[CrossRef](#)]

29. Devkota, K.C.; Regmi, A.D.; Pourghasemi, H.R.; Yoshida, K.; Pradhan, B.; Ryu, I.C.; Dhital, M.R.; Althuwaynee, O.F. Landslide susceptibility mapping using certainty factor, index of entropy and logistic regression models in GIS and their comparison at Mugling–Narayanghat road section in Nepal Himalaya. *Nat. Hazards* **2013**, *65*, 135–165. [[CrossRef](#)]
30. Chen, W.; Liu, S. Microstructural topology optimization of viscoelastic materials for maximum modal loss factor of macrostructures. *Struct. Multidiscip. Optim.* **2016**, *53*, 1–14. [[CrossRef](#)]
31. Zêzere, J.L.; Pereira, S.; Melo, R.; Oliveira, S.C.; Garcia, R.A.C. Mapping landslide susceptibility using data-driven methods. *Sci. Total Environ.* **2017**, *589*, 250–267. [[CrossRef](#)] [[PubMed](#)]
32. Tang, R.-X.; Yan, E.C.; Wen, T.; Yin, X.-M.; Tang, W. Comparison of Logistic Regression, Information Value, and Comprehensive Evaluating Model for Landslide Susceptibility Mapping. *Sustainability* **2021**, *13*, 3803. [[CrossRef](#)]
33. Lee, S.; Ryu, J.-H.; Min, K.; Won, J.-S. Landslide susceptibility analysis using GIS and artificial neural network. *Earth Surf. Process. Landf.* **2003**, *28*, 1361–1376. [[CrossRef](#)]
34. Pham, B.T.; Tien Bui, D.; Dholakia, M.B.; Prakash, I.; Pham, H.V. A Comparative Study of Least Square Support Vector Machines and Multiclass Alternating Decision Trees for Spatial Prediction of Rainfall-Induced Landslides in a Tropical Cyclones Area. *Geotech. Geol. Eng.* **2016**, *34*, 1807–1824. [[CrossRef](#)]
35. Yilmaz, I. The effect of the sampling strategies on the landslide susceptibility mapping by conditional probability and artificial neural networks. *Environ. Earth Sci.* **2010**, *60*, 505–519. [[CrossRef](#)]
36. Mallick, J.; Alqadhi, S.; Talukdar, S.; AlSubih, M.; Ahmed, M.; Khan, R.A.; Kahla, N.B.; Abutayeh, S.M. Risk Assessment of Resources Exposed to Rainfall Induced Landslide with the Development of GIS and RS Based Ensemble Metaheuristic Machine Learning Algorithms. *Sustainability* **2021**, *13*, 457. [[CrossRef](#)]
37. Chen, W.; Xu, S.; Zou, Y. Stabilization of hybrid neutral stochastic differential delay equations by delay feedback control. *Syst. Control Lett.* **2016**, *88*, 1–13. [[CrossRef](#)]
38. Colkesen, I.; Sahin, E.K.; Kavzoglu, T. Susceptibility mapping of shallow landslides using kernel-based Gaussian process, support vector machines and logistic regression. *J. Afr. Earth Sci.* **2016**, *118*, 53–64. [[CrossRef](#)]
39. Xu, C.; Dai, F.; Xu, X.; Lee, Y.H. GIS-based support vector machine modeling of earthquake-triggered landslide susceptibility in the Jianjiang River watershed, China. *Geomorphology* **2012**, *145–146*, 70–80. [[CrossRef](#)]
40. Hong, H.; Pourghasemi, H.R.; Pourtaghi, Z.S. Landslide susceptibility assessment in Lianhua County (China): A comparison between a random forest data mining technique and bivariate and multivariate statistical models. *Geomorphology* **2016**, *259*, 105–118. [[CrossRef](#)]
41. Park, S.; Hamm, S.-Y.; Kim, J. Performance Evaluation of the GIS-Based Data-Mining Techniques Decision Tree, Random Forest, and Rotation Forest for Landslide Susceptibility Modeling. *Sustainability* **2019**, *11*, 5659. [[CrossRef](#)]
42. Costanzo, D.; Chacón, J.; Conoscenti, C.; Irigaray, C.; Rotigliano, E. Forward logistic regression for earth-flow landslide susceptibility assessment in the Platani river basin (Southern Sicily, Italy). *Landslides* **2014**, *11*, 639–653. [[CrossRef](#)]
43. Lee, S. Comparison of landslide susceptibility maps generated through multiple logistic regression for three test areas in Korea. *Earth Surf. Process. Landf.* **2007**, *32*, 2133–2148. [[CrossRef](#)]
44. Nourani, V.; Pradhan, B.; Ghaffari, H.; Sharifi, S.S. Landslide susceptibility mapping at Zonouz Plain, Iran using genetic programming and comparison with frequency ratio, logistic regression, and artificial neural network models. *Nat. Hazards* **2014**, *71*, 523–547. [[CrossRef](#)]
45. Chen, W.; Xie, X.; Wang, J.; Pradhan, B.; Hong, H.; Bui, D.T.; Duan, Z.; Ma, J. A comparative study of logistic model tree, random forest, and classification and regression tree models for spatial prediction of landslide susceptibility. *Catena* **2017**, *151*, 147–160. [[CrossRef](#)]
46. Fan, W.; Wei, X.S.; Cao, Y.B.; Zheng, B. Landslide susceptibility assessment using the certainty factor and analytic hierarchy process. *J. Mt. Sci.* **2017**, *14*, 906–925. [[CrossRef](#)]
47. Cao, Y.; Jia, H.; Xiong, J.; Cheng, W.; Li, K.; Pang, Q.; Yong, Z. Flash Flood Susceptibility Assessment Based on Geodetector, Certainty Factor, and Logistic Regression Analyses in Fujian Province, China. *Isprs Int. J. Geo-Inf.* **2020**, *9*, 748. [[CrossRef](#)]
48. Chen, W.; Zhang, S.; Li, R.; Shahabi, H. Performance evaluation of the GIS-based data mining techniques of best-first decision tree, random forest, and naïve Bayes tree for landslide susceptibility modeling. *Sci. Total Environ.* **2018**, *644*, 1006–1018. [[CrossRef](#)]
49. Pandey, V.K.; Pourghasemi, H.R.; Sharma, M.C. Landslide susceptibility mapping using maximum entropy and support vector machine models along the highway corridor, Garhwal Himalaya. *Geocarto Int.* **2018**, *35*, 168–187. [[CrossRef](#)]
50. Zheng, D.; Frost, J.D.; Huang, R.Q.; Liu, F.Z. Failure process and modes of rockfall induced by underground mining: A case study of Kaiyang Phosphorite Mine rockfalls. *Eng. Geol.* **2015**, *197*, 145–157. [[CrossRef](#)]
51. Conoscenti, C.; Ciaccio, M.; Caraballo-Arias, N.A.; Gómez-Gutiérrez, Á.; Rotigliano, E.; Agnesi, V. Assessment of susceptibility to earth-flow landslide using logistic regression and multivariate adaptive regression splines: A case of the Belice River basin (Western Sicily, Italy). *Geomorphology* **2015**, *242*, 49–64. [[CrossRef](#)]
52. Hong, H.; Chen, W.; Xu, C.; Youssef, A.M.; Pradhan, B.; Tien Bui, D. Rainfall-induced landslide susceptibility assessment at the Chongren area (China) using frequency ratio, certainty factor, and index of entropy. *Geocarto Int.* **2016**, 1–16. [[CrossRef](#)]
53. Hussain, G.; Singh, Y.; Bhat, G.M. Landslide Susceptibility Mapping along the National Highway-1D, between Kargil and Lamayuru, Ladakh Region, Jammu and Kashmir. *J. Geol. Soc. India* **2018**, *91*, 457–466. [[CrossRef](#)]
54. Chen, Z.; Song, D.; Juliev, M.; Pourghasemi, H.R. Landslide susceptibility mapping using statistical bivariate models and their hybrid with normalized spatial-correlated scale index and weighted calibrated landslide potential model. *Environ. Earth Sci.* **2021**, *80*. [[CrossRef](#)]

55. Aditian, A.; Kubota, T.; Shinohara, Y. Comparison of GIS-based landslide susceptibility models using frequency ratio, logistic regression, and artificial neural network in a tertiary region of Ambon, Indonesia. *Geomorphology* **2018**, *318*, 101–111. [[CrossRef](#)]
56. Çevik, E.; Topal, T. GIS-based landslide susceptibility mapping for a problematic segment of the natural gas pipeline, Hendek (Turkey). *Environ. Geol.* **2003**, *44*, 949–962. [[CrossRef](#)]
57. Duan, G.; Zhang, J.; Zhang, S. Assessment of Landslide Susceptibility Based on Multiresolution Image Segmentation and Geological Factor Ratings. *Int. J. Environ. Res. Public Health* **2020**, *17*, 7863. [[CrossRef](#)]
58. Bucci, F.; Santangelo, M.; Cardinali, M.; Fiorucci, F.; Guzzetti, F. Landslide distribution and size in response to Quaternary fault activity: The Peloritani Range, NE Sicily, Italy. *Earth Surf. Process. Landf.* **2016**, *41*, 711–720. [[CrossRef](#)]
59. Chen, C.Y.; Huang, W.L. Land use change and landslide characteristics analysis for community-based disaster mitigation. *Environ. Monit. Assess* **2013**, *185*, 4125–4139. [[CrossRef](#)]
60. Zhang, H.; Chi, T.; Fan, J.; Hu, K.; Peng, L. Spatial Analysis of Wenchuan Earthquake-Damaged Vegetation in the Mountainous Basins and Its Applications. *Remote Sens.* **2015**, *7*, 5785–5804. [[CrossRef](#)]
61. O'Brien, R.M. A Caution Regarding Rules of Thumb for Variance Inflation Factors. *Qual. Quant.* **2007**, *41*, 673–690. [[CrossRef](#)]
62. Djukem, W.D.L.; Braun, A.; Wouatong, A.S.L.; Guedjeo, C.; Dohmen, K.; Wotchoko, P.; Fernandez-Steeger, T.M.; Havenith, H.B. Effect of Soil Geomechanical Properties and Geo-Environmental Factors on Landslide Predisposition at Mount Oku, Cameroon. *Int. J. Environ. Res. Public Health* **2020**, *17*, 6795. [[CrossRef](#)]
63. Xiong, J.; Ye, C.; Cheng, W.; Guo, L.; Zhou, C.; Zhang, X. The Spatiotemporal Distribution of Flash Floods and Analysis of Partition Driving Forces in Yunnan Province. *Sustainability* **2019**, *11*, 2926. [[CrossRef](#)]
64. Booth, G.D.; Niccolucci, M.J.; Schuster, E.G.; Station, I. Identifying proxy sets in multiple linear-regression—An aid to better coefficient interpretation. *J. Appl. Physiol.* **1994**, *89*, 807–822. [[CrossRef](#)]
65. Shortliffe, E.H.; Buchanan, B.G. A model of inexact reasoning in medicine. *Math. Biosci.* **1975**, *23*, 351–379. [[CrossRef](#)]
66. Heckerman, D. Probabilistic Interpretation for MYCIN's Certainty Factors. *Mach. Intell. Pattern Recognit.* **1986**, *4*, 167–196. [[CrossRef](#)]
67. Lan, H.X.; Zhou, C.H.; Wang, L.J.; Zhang, H.Y.; Li, R.H. Landslide hazard spatial analysis and prediction using GIS in the Xiaojiang watershed, Yunnan, China. *Eng. Geol.* **2004**, *76*, 109–128. [[CrossRef](#)]
68. Pourghasemi, H.R.; Moradi, H.R.; Fatemi Aghda, S.M. Landslide susceptibility mapping by binary logistic regression, analytical hierarchy process, and statistical index models and assessment of their performances. *Nat. Hazards* **2013**, *69*, 749–779. [[CrossRef](#)]
69. Saaty, T.L.; Kearns, K.P. Systems Characteristics and The Analytic Hierarchy Process. *Anal. Plan.* **1985**, *4*, 63–86. [[CrossRef](#)]
70. Ayalew, L.; Yamagishi, H.; Marui, H.; Kanno, T. Landslides in Sado Island of Japan: Part II. GIS-based susceptibility mapping with comparisons of results from two methods and verifications. *Eng. Geol.* **2005**, *81*, 432–445. [[CrossRef](#)]
71. Saaty, T.L. Analytic hierarchy process. In *Encyclopedia of Operations Research and Management Science*; Gass, S.I., Harris, C.M., Eds.; Springer: New York, NY, USA, 2001; pp. 19–28. [[CrossRef](#)]
72. Saaty, T.L. A scaling method for priorities in hierarchical structures. *J. Math. Psychol.* **1977**, *15*, 234–281. [[CrossRef](#)]
73. Ayalew, L.; Yamagishi, H. The application of GIS-based logistic regression for landslide susceptibility mapping in the Kakuda-Yahiko Mountains, Central Japan. *Geomorphology* **2005**, *65*, 15–31. [[CrossRef](#)]
74. Van Den Eeckhaut, M.; Vanwallegem, T.; Poesen, J.; Govers, G.; Verstraeten, G.; Vandekerckhove, L. Prediction of landslide susceptibility using rare events logistic regression: A case-study in the Flemish Ardennes (Belgium). *Geomorphology* **2006**, *76*, 392–410. [[CrossRef](#)]
75. Nefeslioglu, H.A.; Gokceoglu, C.; Sonmez, H. An assessment on the use of logistic regression and artificial neural networks with different sampling strategies for the preparation of landslide susceptibility maps. *Eng. Geol.* **2008**, *97*, 171–191. [[CrossRef](#)]
76. Bai, S.-B.; Wang, J.; Lü, G.-N.; Zhou, P.-G.; Hou, S.-S.; Xu, S.-N. GIS-based logistic regression for landslide susceptibility mapping of the Zhongxian segment in the Three Gorges area, China. *Geomorphology* **2010**, *115*, 23–31. [[CrossRef](#)]
77. Hosmer, D.; Lemeshow, S. Addendum. *Appl. Logist. Regres.* **2000**, 354. [[CrossRef](#)]